Correlated electron behavior of metal-organic molecules: Insights from density functional theory combined with many-body effects using exact diagonalization

Sumanta Bhandary,[1,*] Malte Schüler,[2,3] Patrik Thunström,[4] Igor di Marco,[1] Barbara Brena,[1] Olle Eriksson,[1] Tim Wehling,[2,3] and Biplab Sanyal[1,†]

[1]*Department of Physics and Astronomy, Uppsala University, Box 516, 751 20 Uppsala, Sweden*

[2]*Institute for Theoretical Physics, University of Bremen, Otto-Hahn-Allee 1, 28359 Bremen, Germany*

[3]*Bremen Center for Computational Materials Science, University of Bremen, Am Falturm 1, 28359 Bremen, Germany*

[4]*Institute of Solid State Physics, Vienna University of Technology, Wiedner Hauptstrasse 8-10, 1040 Wien, Austria*

(Received 30 May 2015; revised manuscript received 7 April 2016; published 27 April 2016)

A proper theoretical description of the electronic structure of the 3*d* orbitals in the metal centers of functional metalorganics is a challenging problem. We apply density functional theory and an exact diagonalization method in a many-body approach to study the ground-state electronic configuration of an iron porphyrin (FeP) molecule. Our study reveals that the consideration of multiple Slater determinants is important, and FeP is a potential candidate for realizing a spin crossover due to a subtle balance of crystal-field effects, on-site Coulomb repulsion, and hybridization between the Fe-*d* orbitals and ligand N-*p* states. The mechanism of switching between two close-lying electronic configurations of Fe-*d* orbitals is shown. We discuss the generality of the suggested approach and the possibility to properly describe the electronic structure and related low-energy physics of the whole class of correlated metal-centered organometallic molecules.

DOI: 10.1103/PhysRevB.93.155158

Molecular magnets combine low dimensionality and inherent confinement effects with strong electron correlations and hold prospects in the context of spintronics. An important molecular property is bistability, i.e., the possibility of realizing two different spin states, which can in principle be accessed and manipulated externally. This is important as the switching of spin has a pronounced effect on measurable quantities, such as magnetic anisotropy and spin dipole moment contribution [1]. Finding ways for the efficient manipulation of the magnetic state [1–4] of transition-metal (TM)-centered porphyrin (TM-P) and phthalocyanine (TM-Pc) molecules has critical consequences in this regard. A crucial interplay between a molecular ligand field and spin pairing energy makes only a subspace of this class of materials to respond to spin crossover.

The magnetic properties in TM-P/TM-Pc are largely governed by the metal center, which features sizable local Coulomb interactions ($U \sim 4$ eV and $J \sim 1$ eV) and is simultaneously subjected to crystal fields, spin-orbit coupling, and orbitally dependent hybridization with the ligands. Electronic correlations are expected to arise [5] and the description by local density approximation (LDA) or generalized gradient approximation (GGA) thus potentially becomes inadequate, for example, leading to an underestimated or even vanishing HOMO-LUMO (highest occupied molecular orbital and lowest unoccupied molecular orbital) gap. Hence, the treatment of the molecular electronic structure in terms of correlated electron theories, such as ligand field theories or Anderson impurity models, becomes crucial. These model-based approaches can be very helpful to trace the physical origin of phenomena such as spin-state switching [5], emergence of magnetic anisotropies [6], or many-body resonances [7], as soon as solid links between the model and the realistic structure can be established. It is worth mentioning that Chiesa *et al.* [8] have demonstrated a similar density functional theory (DFT)-based method to construct many-body Hamiltonians using Foster-Boys molecular orbitals to describe the magnetic properties of molecular nanomagnets.

In this paper, we have adapted a hybrid approach [9] (DFT++), which links density functional theory (DFT) and Anderson's impurity model to study the physical properties of FeP and FePc. We demonstrate how the interplay of Coulomb interactions, crystal fields, and hybridization with the ligands, which are fully captured in our theory, leads to correlated electron physics, and how this theory describes the $S = 1 \rightarrow S = 2$ spin crossover in the Fe^{2+} metal center of FeP. Furthermore, the crossover between different close-lying ground-state electronic configurations within the $S = 1$ subspace of the correlated Fe-*d* orbitals is analyzed.

The problem can be cast in the following way. The delocalized orbitals in the organic ring in FeP are described by LDA or GGA, but the Fe center is considered as an impurity embedded in the organic host and is described by Anderson's impurity model [10].

The model Hamiltonian for the impurity problem can be expressed as

$$H = \sum_{i,j} \epsilon^d_{ij} d^\dagger_i d_j + \frac{1}{2} \sum_{i,j,k,l} U_{ijlk} d^\dagger_i d^\dagger_j d_k d_l + \sum_{ik} (V_{ik} c^\dagger_k d_i + \text{H.c.}) + \sum_k \epsilon_k c^\dagger_k c_k, \quad (1)$$

where ϵ^d_{ij} describes the on-site energies and $i,j,k,l = (m,\sigma)$ represent combined orbital and spin indices. d_i is the annihilation operator, while U_{ijlk} represents the local Coulomb interaction. U_{ijlk} is parametrized by Slater parameters. We have chosen $U = 4$ eV and $J = 1$ eV for $l = 2$ (3*d* orbitals) in our calculations; see Supplemental Material [16] for details.

*Present address: Institute of Solid State Physics, Vienna University of Technology, Wiedner Hauptstrasse 8-10, 1040 Wien, Austria.

†biplab.sanyal@physics.uu.se

 ©2016 American Physical Society

In the above equation, the first two terms represent electrons in Fe-3*d* orbitals. The third term describes the interaction with the surrounding atoms, while the fourth term is for the delocalized ligand electrons with energies ϵ_k. The hopping matrix element V_{ik} appears in the hybridization function, which is represented as

$$\Delta_{ij}(\epsilon) = \sum_k \frac{V_{ik} V_{kj}}{\epsilon + i\delta - \epsilon_k}. \quad (2)$$

The energy-dependent hybridization function can be obtained from first-principles calculations. We follow the approach considered by Karolak *et al.* [9] to construct the local Green's function from DFT. The Kohn-Sham Green's function G_{KS} can be calculated from the Lehmann representation [11] using

$$G_{KS}(\epsilon) = \sum_{nk} \frac{|\psi_{nk}\rangle \langle \psi_{nk}|}{\epsilon + i\delta - \epsilon_{nk}}, \quad (3)$$

where ψ_{nk}'s and ϵ_{nk}'s are the Kohn-Sham eigenstates and eigenvalues for band n and reciprocal space point k. The projection of the full Green's function to an atom-centered local Green's function $G^{mm'}_{\text{imp}}$ for localized orbitals is needed, which in our case are cubic harmonics (χ_m),

$$G^{mm'}_{\text{imp}}(\epsilon) = \sum_{nk} \frac{P^m_{nk} P^{m'*}_{nk}}{\epsilon + i\delta - \epsilon_{nk}}, \quad (4)$$

where $P^m_{nk} = \langle \chi_m \mid \psi_{nk} \rangle$ and $P^{m'*}_{nk} = \langle \psi_{nk} \mid \chi_{m'} \rangle$. The hybridization function is calculated from the local impurity Green's function from the expression

$$G^{-1}_{\text{imp}}(\epsilon) = \epsilon + i\delta - E_{\text{cryst}} - \Delta(\epsilon) = \epsilon + i\delta - \tilde{\Delta}(\epsilon). \quad (5)$$

In the above expression, G_{imp} is the projected Green's function on local orbitals and $\tilde{\Delta}$ combines the hybridization function Δ and static crystal field E_{cryst}. If the bath orbitals [defined by ϵ_k and V_{ik} in Eq. (2)] are limited to a small number of discrete orbitals only, the many-body problem defined in Eq. (1) can be solved by means of exact diagonalization (ED), which will be used here.

Electrons in Fe-3*d* orbitals hybridize mostly with the orbitals of the four surrounding N atoms, which provide a square planar ligand field. The effect of the outer C-ring is rather indirect as that mainly shifts N-*p* levels by both in-plane and π-π interaction. The energy dependence of that interaction with surrounding N atoms can be described by an energy-dependent hybridization function $\tilde{\Delta}(\epsilon)$. We have employed non-spin-polarized density functional calculations within local density and generalized gradient approximations to extract the hybridization functions. The DFT calculations were performed using the VASP code [12] that employs a plane-wave basis and projector augmented wave method. In Fig. 1, real and imaginary parts of $\tilde{\Delta}$ are shown. The imaginary part (Im$\tilde{\Delta}$) quantifies the density of bath states coupling to each impurity orbital weighted by the hybridization matrix elements V_{ik}. As seen from Fig. 1, the most dominant peak in Im$\tilde{\Delta}(\epsilon)$ is observed for the Fe-$d_{x^2-y^2}$ orbital at 2.03 eV below the Fermi energy. The formation of in-plane σ bonds with axial N ligands explains this pronounced peak. It should be noted that the other in-plane orbital d_{xy} shows almost no hybridization, apart from a small peak at 4.8 eV below the

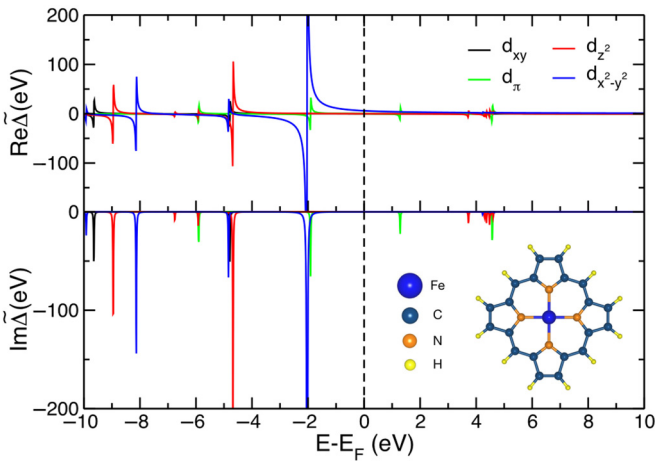

FIG. 1. Real and imaginary parts of the hybridization function for Fe in FeP calculated with PBE in the non-spin-polarized mode. A smearing parameter of 0.01 eV has been used for this plot for the sake of visualization. The geometry of FeP is shown in the inset with the atoms labeled by their types.

Fermi energy. The out-of-plane orbitals have relatively small peaks in Im$\tilde{\Delta}$, among which the one closest to the Fermi energy is of d_π (d_{xz}, d_{yz}) character at -2 eV. The appearance of this peak reflects a π-π interaction of Fe-d_π orbitals with N-p_z orbitals, which is expected in the square planar ligand field of the FeP molecule. The other out-of-plane and in-plane contributions are present in the -4.5 to -10 eV energy range. Taken together, the hybridization function reveals a strong in-plane interaction between Fe-$d_{x^2-y^2}$ orbitals and the N-*p* ligand states along with a much weaker interaction among all other orbitals.

The real part of the hybridization function Re$\tilde{\Delta}$ describes the energy-dependent ligand field, combined with a static crystal field, which can be obtained at the $\epsilon \to \infty$ limit. The strong resonance with the host and $d_{x^2-y^2}$ orbital manifests itself also around -2.03 eV in Re$\tilde{\Delta}$. This strong ligand field pushes $d_{x^2-y^2}$ high in energy, causing almost no occupancy in either spin channel. In the gas phase, six electrons in Fe^{2+} thus are distributed in the remaining four *d* orbitals, with four and two electrons in the majority and minority spin channels, respectively, giving rise to an intermediate spin state ($S = 1$).

An intriguing phenomenon of strain-induced spin state switching is observed theoretically in FeP [1,3,13], which is relatively difficult to obtain for other molecules with other TM centers [14,15] or different structures, e.g., transition-metal phthalocyanines. Iron phthalocyanine (FePc), for example, has an Fe center but also a larger organic ring. This results in a stronger hybridization of Fe with the neighboring N atoms (shown in the Supplemental Material (SM) [16]), which is reflected in the appearance of a $d_{x^2-y^2}$ peak in Im$\tilde{\Delta}$ at -1.86 eV and a stronger hybridization (3.67 eV). The shift of the bath energy to -1.86 eV for FePc compared to -2.03 eV in FeP is due to the presence of four extra N atoms connected to the pyrolle rings in FePc (see Fig. 2 in the SM [16]). These four N atoms are not directly bonded to Fe, but are connected to N atoms in the Fe-N_4 block via C atoms.

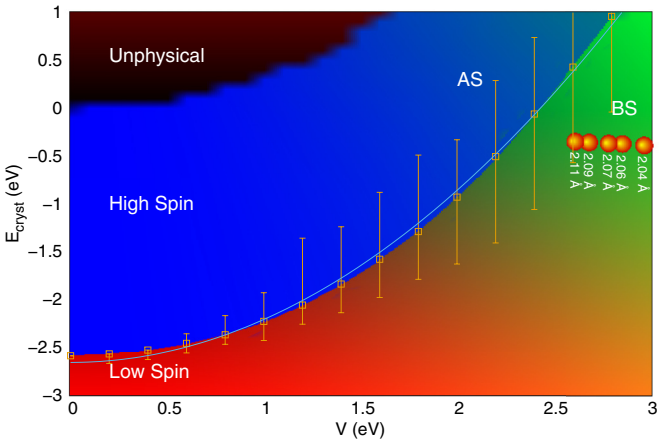

FIG. 2. The phase diagram depicting the spin states of FeP with the tuning of the static crystal field E_{cryst} and the hybridization strength V. The phase boundary is accompanied by the allowed values of E_{cryst} for fixed values of V. The blue curve is a result of fitting with a tight-binding model described in the Supplemental Material [16]. AS and BS indicate antibonding and bonding regions. Calculated values of E_{cryst} and V from DFT (non-spin-polarized PBE) are shown in orange circles along with the corresponding Fe-N bond lengths.

To quantify the conditions required for spin-state switching of FeP, we have constructed a phase diagram by varying crystal field and hybridization strength within the DFT++ method. The variation of these parameters mimics the strain effect on the molecule. Also, as mentioned in the previous section, we found that the crystal-field splitting of $d_{x^2-y^2}$ is larger compared to other orbitals and, as discussed below, this splitting is responsible for the spin switching. For this part of the calculation, we have kept a common reference level of the rest of the orbitals separated from $d_{x^2-y^2}$ by E_{cryst}, which was varied. An independent variation of the hopping matrix elements, $V_{d_{x^2-y^2}}$, is done along with the variation of E_{cryst}. One needs to keep in mind that for our model calculation, E_{cryst} and $V_{d_{x^2-y^2}}$ are independent, while in DFT calculation, these parameters are implicitly related. The ligand field variation due to the strain effect simultaneously changes E_{cryst} and $V_{d_{x^2-y^2}}$. For the remaining part of the discussion, we will refer to $V_{d_{x^2-y^2}}$ as V, as this is the only bath-site coupling considered for our model calculations.

Figure 2 depicts the spin phase diagram of the central atom in FeP. The phases are defined by the characteristic energy contributions and demonstrated with the red-green-blue (RGB) color code (see Supplemental Material [16]). For $V \to 0$ and with sufficiently high crystal field ($E_{\text{cryst}} > 2.6$ eV), six electrons occupy the degenerate d_{rest} level. Hence, the ground state will be a low-spin state with an energy gain from the crystal field (red), but with the cost of exchange energy (blue). The ground state attains a high-spin state for low crystal fields. A strong V pushes the molecular orbital containing predominantly $d_{x^2-y^2}$ and, hence, the required crystal field for spin crossover is small. The intermediate spin state, in this situation, is governed by the Fe-N bonding (green). The crystal field can be tuned to occupy the antibonding molecular orbital and, hence, the $S = 2$ spin state can be achieved (denoted AS in Fig. 2). The dependence of V on E_{cryst} follows a quadratic behavior. The fitted curve in Fig. 2 at the phase boundary is obtained from a mean-field model (see Supplemental Material [16]) containing one particle Hamiltonian, but with a renormalized on-site energy ϵ^d. The discrepancy between the phase boundary and the fitted curve lies in proper renormalization of ϵ^d, which depends linearly with N, by electron correlation energy, which has a dependence of N^2.

As the spectrum of the FeP molecule is gapped, we placed chemical potential in the middle of the gap. But it is also possible to vary the average on-site d energy ϵ_d, while keeping the total number of particles in the system fixed. In addition, the average d-electron on-site energy is not exactly known from the DFT simulations—a problem usually referred to as the *double-counting problem* in the DFT++, DFT+U, or DFT+DMFT (dynamical mean-field theory) approaches. In our case, this means that the average on-site energy or, more precisely, the average energy difference between the bath level and the Fe-d block carries some uncertainty. We thus vary ϵ_d in a range, while keeping the total number of particles in our system constant. In this way, the high-spin to low-spin transition line has error bars associated with some of the calculated points shown in Fig. 2.

At a stronger coupling V, the shifting of the on-site energy ϵ_d will allow a variation of E_{cryst}, where a spin crossover (SCO) can happen. The range of E_{cryst} due to the variation of ϵ_d is presented by the orange error bars in Fig. 2. In the regime of weak hybridization, the system is described predominantly by crystal fields. There are, in particular, no charge fluctuations to $N = 7$ or $N = 5$ Fe impurity states, which are generally affected by changing ϵ_d. As there is no mixing with $N \neq 6$ impurity states in the limit of $V \to 0$, the error bar is vanishingly small in this limit. For V beyond 2.8 eV, this particular scenario of crystal field will not be able to switch the spin state. An orbital reversal, i.e., the $d_{x^2-y^2}$ energy becoming lowered compared to other orbitals, is needed in this case, which requires a different kind of charge distribution in the molecule. Thus, a transition between the $S = 1$ and $S = 2$ states could be realized for $V < 2.8$ eV, while $S = 1$ should be obtained generally for $V > 2.8$ eV.

Weakening of the ligand field leading to a spin-state change, however, needs a nontrivial chemical or physical procedure. The existence of high-spin ($S = 2$) porphyrin complexes with d^6 configuration has so far been observed in nonplanar molecules with five or six coordination of the central Fe atom [17]. Higher coordination leads to an out-of-plane shift of the central Fe atom (five coordination) or symmetrical Fe-N block expansion, resulting in a weaker ligand field. For four coordination, however, the $S = 2$ state is yet to be confirmed experimentally. Figure 2 establishes the parameter space for when this state is to be expected.

The variation of V is also studied with Perdew-Burke-Ernzerhof (PBE) by varying the Fe-N bond length in the molecule. The highest value of V (3.36 eV) is obtained for a Fe-N bond length of 1.97 Å. The five data points, shown in Fig. 2 in filled orange circles, are for bond lengths in the range of 2.04 to 2.11 Å. As mentioned in Refs. [1,3] for FeP either physisorbed or chemisorbed on surfaces, the required bond length of Fe-N in FeP for spin switching is beyond 2.04 Å within the PBE+U approximation with $U_{\text{eff}} = 3$ eV [18]. This

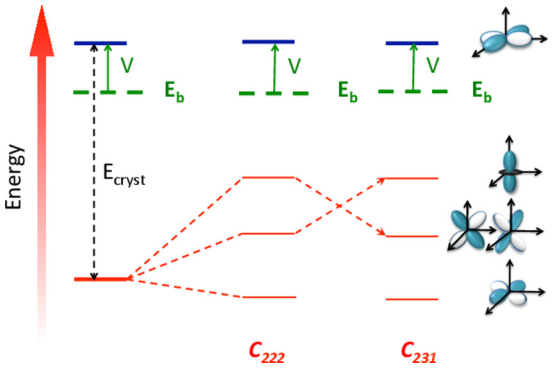

FIG. 3. Schematic diagram depicting the C_{222} and C_{231} configurations. E_{cryst} describes the energy separation between $d_{x^2-y^2}$ and the rest of the d orbitals treated as degenerate. V denotes the strength of hybridization between the $d_{x^2-y^2}$ and the bath state with an energy E_b. The specific orbitals corresponding to the occupation of the energy levels are also indicated.

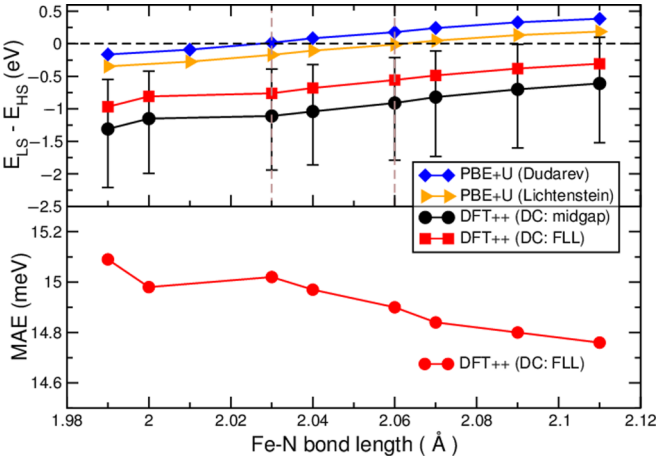

FIG. 4. Upper panel: Energy differences between low-spin (LS) and high-spin (HS) states calculated by DFT++ [double counting (DC) treated by placing chemical potential in the middle of the gap and DC calculated using the fully localized limit (FLL)] and PBE+U (double counting by Dudarev and Lichtenstein) methods as a function of Fe-N bond lengths in FeP. The error bars correspond to the variation of on-site energy [model Hamiltonian in Eq. (1)] in DFT++ calculations. Lower panel: Magnetic anisotropy energy (MAE) as a function of Fe-N bond lengths calculated with the double-counting correction in the fully localized limit.

is in agreement with the data shown in Fig. 2, where both DFT++ and PBE suggest a spin crossover beyond 2.04 Å. A detailed comparison between the bond lengths required for spin crossover in PBE+U and DFT++ is shown in Fig. 3. A comparison of PBE and LDA calculations yields values of the static crystal field, bath energy, and hybridization as 0.42 (0.37) eV, −2.03 (−1.89) eV, and 3.36 (3.63) eV for PBE (LDA).

The free-molecule spin state ($S = 1$) is particularly interesting from the point of view of the ground-state configuration. A strong ligand field in the free molecule leaves $d_{x^2-y^2}$ nearly unoccupied and an intermediate spin state ($S = 1$) can have a ground-state electronic configuration with two electrons in d_{xy}, three electrons in d_π, and one electron in d_{z^2}. We will refer to this configuration as a C_{231} ($d^2_{xy}d^3_\pi d^1_{z^2}$) configuration. The other possible configurations within the $S = 1$ ground-state multiplet are C_{222} ($d^2_{xy}d^2_\pi d^2_{z^2}$), C_{141} ($d^1_{xy}d^4_\pi d^1_{z^2}$), and C_{132} ($d^1_{xy}d^3_\pi d^2_{z^2}$), among which the C_{222} appears to be very close in energy to the energy of C_{231}. From $\text{Re}\tilde{\Delta}$, a splitting can also be seen among d_π, d_{z^2}, and d_{xy} orbitals, but in a relatively small energy scale. To acquire a clear view of the ground-state configuration, we varied the crystal field in the presence and absence of coupling V. In the first step, we only considered a crystal-field splitting between $d_{x^2-y^2}$ and the averaged position of the remaining orbitals, as shown in the leftmost part of Fig. 3. In this pure crystal-field situation, the $S = 1$ state leads to the C_{231} ground-state configuration. As the coupling V is switched on, the ground-state configuration becomes on-site energy dependent. This happens because the inclusion of strong hybridization will admix $N = 5$ and $N = 7$ impurity occupancies with the pure $N = 6$ ground-state configuration of the pure crystal-field situation. Varying on-site energy, the ground-state configuration can be modified. The energy scale associated to this change is of the order of meV. A relative splitting among the remaining orbitals has even more pronounced effects in determining the ground-state configuration. As shown in Fig. 3, with additional splitting, if d_π stays above d_{z^2}, C_{222} is stabilized. However, in the reverse situation, C_{231} is obtained. This change occurs in an at least one- or two-order-higher energy scale compared to the many-body-effects-induced configuration change, revealing the crystal field to be the dominant factor from that aspect.

Let us now move on to the realistic calculations, where DFT-extracted V and E_{cryst} are explicitly employed. Apart from $d_{x^2-y^2}$, the relative splitting within the rest of the d orbitals is considered as well. In the upper panel of Fig. 4, a comparison between the spin-crossover properties of FeP as predicted by different flavors of PBE+U and DFT++ is shown. In the PBE+U calculations, we stabilize the nonfavorable spin solutions by constraining the spin moments. First of all, the energy difference between the LS and HS configurations is close for the PBE+U calculations done using the Dudarev and Lichtenstein approaches. However, there is a notable difference between these PBE+U methods in the Fe-N bond length required for the LS-HS transition. Second, the bond lengths required for the spin transition obtained from Lichtenstein PBE+U and DFT++ with the same form of double-counting correction are higher compared to that obtained from the Dudarev method. This is understandable since both the Lichtenstein variant of PBE+U and DFT++ employ the full four-fermion Coulomb matrix as defined through the Slater parameters, whereas Dudarev assumes a simplified Coulomb vertex. DFT++ with two different DC corrections is also expected to yield spin crossover, but with larger strains. The black curve in the upper panel of Fig. 4 represents the choice of double counting that puts chemical potential in the middle of the gap between the $N = 8$ and $N = 7/9$ spectra. The error bars define the situations corresponding to the placement of chemical potentials close to the edges of the gap. The choice of fully localized limit (FLL) of double counting results in the red curve in the upper panel of Fig. 4.

The general difference between the DFT++ and PBE+U approaches in terms of spin-crossover energies is clearly evident from Fig. 4. DFT++ results in multiple Slater determinant states, the evidence of which can be observed from the occupations corresponding to two different spin states. The high-spin ($S = 2$) state exhibits an almost integer occupation, suggesting the presence of a single Slater determinant. In contrast to that, the $S = 1$ solution produces rather fractional occupations, reflecting the presence of multiple Slater determinants. As PBE+U always chooses a single Slater determinant, an additional energy cost is involved. This energy cost is much higher for the $S = 1$ state due to its multiple Slater determinantal nature compared to the $S = 2$ state. This can be clearly seen from the upper panel of Fig. 4, where $E_{LS} - E_{HS}$ for PBE+U is significantly small compared to DFT++, signifying the differences in strain in FeP required to bring about the spin crossover in two cases. In the lower panel of Fig. 3, the calculated magnetic anisotropy energies (MAEs) within DFT++ (with DC correction in FLL) are shown for different Fe-N bond lengths. In all of the cases, we have found the easy axis of magnetization to lie in the plane of the molecule. Our calculated large values of MAE have also been observed in recent experiments [19].

It should be mentioned that convergence tests on spin-transition energy $\Delta E(E_{LS}$-$E_{HS})$ have been performed by increasing the number of bath states per d orbital. The number of bath states for the most important $d_{x^2-y^2}$ orbital is systematically increased from 1 to 4, while the number of bath states for other d orbitals is considered to be 0 and 1. Our DFT++ calculations with four bath states for $d_{x^2-y^2}$ and one bath state for each of the rest of the orbitals result in a minor change (about 3%) in ΔE (see SM [16] for more details). This justifies the validity of our approximation of using a single bath state.

In summary, we have presented ground-state electronic properties of Fe in an FeP molecule with a hybrid approach of DFT combined with a many-body treatment, using exact diagonalization. We have demonstrated that a delicate interplay of the static crystal field, ligand hybridization, and Coulomb interactions promotes iron porphyrin to be a potential candidate for realizing spin-crossover behavior. In general, our calculated phase diagram indicates the possibility of tuning electronic and magnetic properties of organometallic molecules to serve the purpose of molecular electronics and storage devices. Moreover, the long-standing debate regarding the electronic ground-state configuration, e.g., C_{222} vs C_{231}, has been solved by identifying the proper parameters required to switch one to the other, which will have important consequences for the spin dipole moments and magnetic anisotropies, where the energy positions of d orbitals with specific symmetries are important.

B.S. acknowledges Carl Tryggers Stiftelse for financial support. O.E. acknowledges support from VR, the KAW Foundation, eSSENCE. We acknowledge supercomputing allocation from the Swedish National Infrastructure for Computing. T.O.W. and M.S. acknowledge support from the Central Research Development Fund of the University of Bremen and the DFG via FOR 1346.

[1] S. Bhandary, S. Ghosh, H. Herper, H. Wende, O. Eriksson, and B. Sanyal, Phys. Rev. Lett. **107**, 257202 (2011).

[2] H. Wende, M. Bernien, J. Luo, C. Sorg, N. Ponpandian, J. Kurde, J. Miguel, M. Piantek, X. Xu, Ph. Eckhold, W. Kuch, K. Baberschke, P. M. Panchmatia, B. Sanyal, P. M. Oppeneer, and O. Eriksson, Nat. Mater. **6**, 516 (2007); V. A. Dediu, L. E. Hueso, and C. Taliani, *ibid.* **8**, 707 (2009).

[3] S. Bhandary, B. Brena, P. M. Panchmatia, I. Brumboiu, M. Bernien, C. Weis, B. Krumme, C. Etz, W. Kuch, H. Wende, O. Eriksson, and B. Sanyal, Phys. Rev. B **88**, 024401 (2013).

[4] S. Bhandary, O. Eriksson, and B. Sanyal, Sci. Rep. **3**, 3405 (2013).

[5] P. Fazekas, *Lecture Notes on Electron Correlation and Magnetism*, Series in Modern Condensed Matter Physics, Vol. 5 (World Scientific, Singapore, 1999).

[6] J. Honolka, A. A. Khajetoorians, V. Sessi, T. O. Wehling, S. Stepanow, J.-L. Mi, B. B. Iversen, T. Schlenk, J. Wiebe, N. B. Brookes, A. I. Lichtenstein, Ph. Hofmann, K. Kern, and R. Wiesendanger, Phys. Rev. Lett. **108**, 256811 (2012)

[7] S. Gardonio, T. O. Wehling, L. Petaccia, S. Lizzit, P. Vilmercati, A. Goldoni, M. Karolak, A. I. Lichtenstein, and C. Carbone, Phys. Rev. Lett. **107**, 026801 (2011).

[8] A. Chiesa, S. Carretta, P. Santini, G. Amoretti, and E. Pavarini, Phys. Rev. Lett. **110**, 157204 (2013)

[9] M. Karolak, T. O. Wehling, F. Lechermann, and A. I. Lichtenstein, J. Phys.: Condens. Matter **23**, 085601 (2011).

[10] P. W. Anderson, Phys. Rev. **124**, 41 (1961).

[11] E. N. Economou, *Green's Functions in Quantum Physics*, Springer Series in Solid-State Sciences (Springer, New York, 2006).

[12] G. Kresse and J. Hafner, Phys. Rev. B **47**, 558(R) (1993); G. Kresse and J. Furthmüller, *ibid.* **54**, 11169 (1996).

[13] M.-S. Liao and S. Scheiner, J. Chem. Phys. **116**, 3635 (2002); W. R. Scheidt and C. A. Reed, Chem. Rev. **81**, 543 (1981); D. C. Rawlings, M. Gouterman, E. R. Davidson, and D. Feller, Int. J. Quant. Chem. **28**, 773 (1985).

[14] O. Kahn and C. J. Martinez, Science **279**, 44 (1998).

[15] P. Gütlich and H. A. Goodwin, Spin Crossover Trans. Metal Compd. I **233**, 1 (2004).

[16] See Supplemental Material at http://link.aps.org/supplemental/10.1103/PhysRevB.93.155158 for the hybridization functions of stretched FeP and FePc molecules, the analysis of the model Hamiltonian describing the phase diagram, and convergence tests on spin-transition energies with respect to the number of bath states.

[17] C. A. Reed, T. Mashiko, W. R. Scheidt, D. Spartalian, and G. Lang, J. Am. Chem. Soc. **102**, 2302 (1980); J. P. Collman, J. L. Hoard, N. Kim, G. Lang, and C. A. Reed, *ibid.* **97**, 2676 (1975); G. B. Jameson, F. S. Molinaro, J. A. Ibers, J. P. Collman, J. I. Brauman, E. Rose, and K. S. Suslick, *ibid.* **102**, 3224 (1980)

[18] D. A. Scherlis, M. Cococcioni, P. Sit, and N. Marzari, J. Phys. Chem. B **111**, 7384 (2007).

[19] B. W. Heinrich, L. Braun, J. I. Pascual, and K. J. Franke, Nano Lett. **15**, 4024 (2015).